Harnessing Direct(Hetero)Arylation in Pursuit of a Saddle-Shaped Perylene Diimide Tetramer

(Supporting Information)

Josh D. B. Koenig, Audrey Laventure, and Gregory C. Welch [a]*

[a] Department of Chemistry, University of Calgary, 2500 University Drive N.W., Calgary, Alberta, Canada T2N 1N4

* Corresponding Author
Email: gregory.welch@ucalgary.ca;

Phone number: 1-403-210-7603

Keywords: saddle-shaped; perylene diimide; tetramer; direct(hetetro)arylation; DHA

TABLE OF CONTENTS

1.	**Methods and Materials**	**S2–S3**
2.	**Synthetic/Experimental Procedures**	**S4–S5**
3.	**^{1}H & ^{13}C NMR Spectroscopy**	**S6–S9**
4.	**HR MALDI-TOF**	**S10–S11**
5.	**Elemental Analysis & Thermal Properties**	**S12**
6.	**UV-Visible Spectroscopy & X-Ray Diffraction**	**S13–S15**
7.	**Voltammetry**	**S16**
8.	**Density Functional Theory**	**S17**
9.	**OPV Device Optimization**	**S18–S22**
10.	**References**	**S23**

1. Methods and Materials

Materials: Polymer PTB7-Th was purchased from 1-Material. SiliaCat® DPP-Pd was purchased from SiliCycle. All other reactants, reagents, and catalysts were purchased from Sigma-Aldrich or VWR and used without further purification.

CHN Elemental Analysis: Elemental analyses were performed by Johnson Li in the Chemical Instrumentation Facility at the University of Calgary. A Perkin Elmer 2400 Series II CHN Elemental Analyzer was used to obtain CHN data, using ~1.5 mg of sample (with particle sizes ranging between 0.2 and 0.5 mm in diameter).

Nuclear Magnetic Resonance (NMR): ^{1}H and ^{13}C NMR spectroscopy experiments were recorded using either a Bruker Avance III 500 or 600 MHz spectrometer. All experiments were performed in either chloroform-d ($CDCl_3$) or tetrachloroethane-d_2. Chemical shifts (referenced to residual solvent) were reported in parts per million (ppm). Multiplicities were reported as follows: singlet (s), doublets (d), triplets (t), quartet (q), pentet (p), hextet (h), doublet of doublets (dd), doublet of triplets (dt), doublet of quartets (dq), triplet of doublets (td), triplet of triplets (tt), and multiplets (m).

High-resolution MALDI-TOF (HR MALDI-TOF): High-resolution MALDI-TOF mass spectrometry measurements were performed courtesy of Jian Jun (Johnson) Li in the Chemical Instrumentation Facility at the University of Calgary. The sample solution (~ 1 µg/ml in dichloromethane) was mixed with matrix trans2-[3-(4-tert-Butylphenyl)-2-methyl-2-propenylidene]malononitrile (DCTB) solution (~5 mg/ml in methanol). All spectra were acquired using a Bruker Autoflex III Smartbeam MALDI-TOF, set to the positive reflective mode (Na:YAG 355 nm laser settings: laser offset = 62-69; laser frequency = 200Hz; and number of shots = 300). The target used was Bruker MTP 384 ground steel plate target.

UV-Visible Spectroscopy (UV-Vis): All absorption measurements were recorded using Agilent Technologies Cary 60 UV-Vis spectrometer at room temperature. All solution UV-Vis spectra were measured with 2 mm quartz cuvettes, using CH_2Cl_2 as solvent. Stock solutions (1.0 mg/mL) of each compound were prepared, serially diluted to concentrations between 10^{-5} - 10^{-6} M, and then used to construct calibration curves for determining molar absorptivity. Variable-temperature measurements were performed using an Agilent Technologies Cary single cell Peltier accessory. Neat films were prepared by spin-coating from a 1 % wt/v solution onto clean Corning glass micro slides. Prior to use, glass slides were cleaned with soap and water, acetone and isopropanol, and followed by UV/ozone treatment using a Novascan UV/ozone cleaning system.

Photoluminescence (PL): All emission measurements were recorded using an Agilent Technologies Cary Eclipse fluorescence spectrophotometer at room temperature.

Atomic Force Microscopy (AFM): AFM measurements were performed by using a TT2-AFM (AFM Workshop) in tapping mode and WSxM software with an 0.01-0.025 Ohm/cm Sb (n) doped Si probe with a reflective back side aluminum coating. Samples for AFM measurement were the same ones that were used to collect the respective the device parameters.

X-Ray Diffraction (XRD): All X-ray diffraction experiments were performed with a PROTO AXRD Benchtop Powder Diffractometer using θ-2θ scans and Cu K-α radiation

Cyclic Voltammetry (CV): Electrochemical measurements were performed using a CH Instruments Inc. Model 1200B Series Handheld Potentiostat. A standard 3-electrode setup was utilized, consisting of a freshly polished glassy carbon disk working electrode (WE), Pt-wire counter electrode (CE), and Ag-wire pseudo-reference electrode (RE). All measurements were referenced to ferrocene ($Fc^{+/0}$) as internal standard. All cyclic voltammetry experiments were performed at a scan rate of 100 mV/s. Sample solutions, with 1 mM compound and 0.1 M tetrabutylammonium hexafluorophosphate ($TBAPF_6$) supporting electrolyte, were prepared in anhydrous CH_2Cl_2. All electrochemical solutions were sparged with dry gas (either N_2 or argon) for 5 minutes to deoxygenate the system prior to measurements. The ionization potentials (IP) and electron affinities (EA) were estimated by correlating the 1st oxidation and 1st reduction potentials ($E_{ox\ 1/2}\ Fc^{0/+}$, $E_{red\ 1/2}\ Fc^{0/+}$) to the normal hydrogen electrode (NHE), assuming the IP of $Fc^{0/+}$ to be 4.80 eV, respectively. [1]

Power Conversion Efficiency (PCE) and External Quantum Efficiency (EQE): The current density-voltage (J-V) curves were measured by a Keithley 2420 source measure unit. The photocurrent was measured under AM 1.5 illumination at 100 mW/cm^2 under a Solar Simulator (Newport 92251A-1000). The standard silicon solar cell (Newport 91150V) was used to calibrate light intensity. EQE was measured in a QEX7 Solar Cell Spectral Response/QE/IPCE Measurement System (PV Measurement, Model QEX7, USA) with an optical lens to focus the light into an area about 0.04 cm^2, smaller than the dot cell. The silicon photodiode was used to calibrate the EQE measurement system in the wavelength range from 300 to 1100 nm.

Organic Photovoltaic (OPV) Devices: Devices were fabricated using ITO-coated glass substrates cleaned by sequentially ultra-sonicating with detergent and de-ionized water, acetone, and isopropanol followed by exposure to UV/ozone for 30 min. ZnO was subsequently deposited as a sol-gel precursor solution in a N_2 purge box following the method of Sun *et al*. [2] The room temperature solution was spin-coated at a speed of 4500 rpm and then annealed at 200 ˚C for at least 15 min. Active layer solutions of PTB7-Th and Th_4PDI_4 were prepared in air with a total concentration of 10-20 mg/mL in *o*-dichlorobenzene (*o*-DCB) with 0-5 % (v/v) 1-chloronaphthalene (CN) additive, unless otherwise noted. Solutions were stirred for 4 h at room temperature. Active layer materials were combined in a 1:1 donor/acceptor weight ratio, unless otherwise noted. The active layer solution was coated at room temperature at a speed of 1000 rpm for 60 s. The substrates with the cast active layers were kept in an N_2 atmosphere glovebox overnight before evaporating MoO_3 and Ag. The 10 nm of MoO_3 followed by 100 nm of Ag were thermally deposited under vacuum (10^{-5} Torr). The active areas of the devices were 0.14 cm^2.

Computational Details: Gas-phase B3LYP/6-31G(d,p) ground-state equilibrium geometry optimizations were considered within Gaussian 09. [3] To reduce the computational cost, all alkyl-substituents were truncated to methyl groups. Molecular dihedral angles were systematically altered to ensure that the optimized geometric structure possessed no imaginary frequencies (at the same level of theory). TD-SCF calculations were also performed from this optimized geometry. Single point calculations were performed on this structure to generate molecular orbitals and electrostatic potential maps.

2. Synthetic/Experimental Procedures

2,5,8,11-tetrakis(trimethylsilyl)cyclooctatetrathiophene (Th_4TMS_4)

TMS_4Th_4 was synthesized by iteratively combining two known literature preparations [4,5].

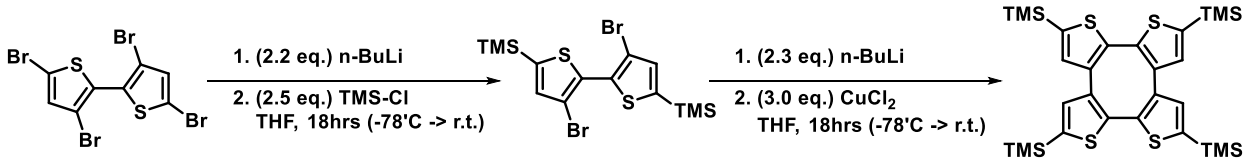

Into a 250 mL Schlenk flask, add 3,3',5,5'-tetrabromobithiophene (2.0g, 4.16 mmol, 1 eq.) and seal the flask with a septum. Complete three vacuum purge and nitrogen backfill cycles on the Schlenk line. Once filled with N_2, cannula transfer over dried THF (80 mL). Stir to dissolve the 3,3',5,5'-tetrabromobithiophene and then cool reaction mixture to -78°C. Dropwise add *n*-butyllithium (3.7 mL, 9.2 mmol, 2.2 eq.) and leave the reaction to stir for 1 hour. Then trimethylsilylchloride (1.3 mL, 10.4 mmol, 2.5 eq.) was added dropwise to the cooled solution and left to stir overnight. The stirring reaction mixture (containing *in-situ* generated intermediate) was cooled to -78°C. *n*-butyllithium (4.0 mL, 9.8 mmol, 2.3 eq.) was dropwise added and left to stir for 1 hour. Under a stream of N_2, the septum was opened and $CuCl_2$ (1.70g, 12.6 mmol, 3 eq.) was added to the reaction. The system was re-sealed and lef to stir overnight. The reaction was quenched with water (75 mL), and then extracted using diethyl ether (3 x 50 mL). Diethyl ether extracts were dried over Na_2SO_4. The drying agent was filtered off and the solvent was concentrated under reduced pressure. The resulting crude oil was purified by silica gel column chromatography (eluted with hexanes) to afford pale yellow solid (452 mg, 0.73 mmol, 35%). The isolated compound matched previously reported spectroscopic properties [5].

Cyclooctatetrathiophene (Th_4)

Th_4 was synthesized using slightly modified literature procedure [6].

Into a 100 mL rbf, Th_4TMS_4 (300 mg, 0.48 mmol, 1 eq.) was dissolved in minimal $CHCl_3$. Trifluoroacetic acid (1 mL, 5.9 mmol, 12 eq.) was added dropwise to the rapidly stirring solution. After 15 minutes, the reaction was quenched by adding H_2O (40 mL). The aqueous mixture was extracted with $CHCl_3$ (3 x 30 mL), and then those extracts were washed with H_2O (2 x 50 mL). After drying organic extracts over Na_2SO_4, the extracts were filtered through Celite and solvent was removed under reduced pressure. Precipitating from MeOH, the resulting off-white solid was collected by vacuum filtration (128 mg, 0.47 mmol, 98%). The isolated compound also matched previously reported spectroscopic properties [6].

^{1}H NMR (500 MHz, $CDCl_3$) δ 7.38 (d, *J* = 5.2 Hz, 4H), 6.97 (d, *J* = 5.2 Hz, 4H).

^{13}C NMR (126 MHz, $CDCl_3$) δ 135.95, 131.78, 129.33, 126.50.

HRMS ($[M]^+$) calculated for M = $C_{16}H_8S_4$: 327.9503.; detected $[M]^+$: 327.9518

Tetrakis(N-hexyl-perylenediimide)cyclooctatetrathiophene (Th_4PDI_4)
Starting material, hexyl-N-perylenediimide bromide (Hex-N-PDI-Br), was synthesized using previously reported literature procedure [7].

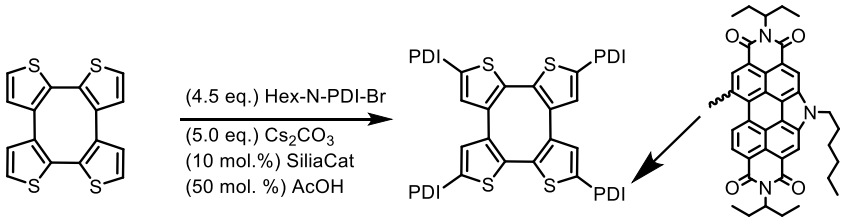

Th_4 (32.8 mg, 0.10 mmol, 1 eq.), Hex-N-PDI-Br (320 mg, 0.45 mmol, 4.5 eq.), Cs_2CO_3 (163 mg, 0.50 mmol, 5 eq.), and SiliaCat-Pd-DPP (0.1 eq., 40 mg, 0.01 mmol) were all added to a 10 mL μwave vial. The vial was sealed and purge with N_2 for 30 minutes. Dried dimethylacetamide (6 mL) was cannula transferred into the vessel and the reaction mixture was sparged for an additional 15 minutes. Acetic acid (3 mg, 0.05 mmol, 0.5 eq.) was injected into the μwave vial and then it was placed in a 120 ºC bead bath for 24 hours. The reaction mixture was poured into methanol (150 mL), stirred for 1 hour, and then vacuum filtered. This crude solid was dissolved in $CHCl_3$, adhered to silica, and further purified by silica gel column chromatography (eluting with $CHCl_3$). The resulting crimson red solid was precipitated into methanol and collected by vacuum filtration. (187 mg, 0.07 mmol, 70%).

^{1}H NMR (600 MHz, tetrachloroethane-d_2, 120 ºC) δ 8.50 (s, 1H, H_{abc}), 8.46 (s, 1H, H_{abc}), 8.41 (s, 1H, H_{abc}), 8.31 (d, *J* = 8.3 Hz, 1H, H_d), 8.00 (d, *J* = 8.3 Hz, 1H, H_e), 7.10 (s, 1H, H_f), 4.64 – 4.57 (m, 1H, H_g), 4.38 (m, 1H, H_h), 4.32 (t, *J* = 7.3 Hz, 2H, H_i), 1.76 (dq, *J* = 15.8, 7.9 Hz, 2H, H_j), 1.69 (p, *J* = 7.4 Hz, 2H, H_k), 1.53 (tt, *J* = 16.1, 8.1 Hz, 2H, H_l), 1.45 (dt, *J* = 14.1, 7.0 Hz, 2H, H_m), 1.28 (dq, *J* = 14.3, 7.4 Hz, 2H, H_n), 0.97 (p, *J* = 7.3 Hz, 2H, H_o), 0.86 (dt, *J* = 15.6, 6.9 Hz, 2H, H_p), 0.78 (dt, *J* = 14.6, 7.2 Hz, 2H, H_q), 0.43 (t, *J* = 7.4 Hz, 6H, H_r), 0.31 (t, *J* = 7.3 Hz, 3H, H_s), 0.24 (dt, *J* = 7.4, 3.5 Hz, 6H, H_t).

^{13}C NMR (151 MHz, tetrachloroethane-d_2, 120 ºC) δ 165.17, 165.09, 163.67, 163.57, 144.89, 137.50, 134.81, 134.68, 134.04, 132.64, 132.55, 131.76, 131.15, 129.51, 127.41, 127.02, 124.47, 124.41, 122.91, 122.78, 122.68, 122.14, 121.82, 121.28, 119.61, 119.51, 118.13, 117.73, 57.70, 57.33, 46.41, 30.74, 30.67, 26.27, 24.88, 24.69, 21.70, 12.98, 10.73, 10.60.

HRMS ($[M+Na]^+$) calculated for M = $C_{176}H_{164}N_{12}O_{16}S_4$: 2852.1163; detected $[M+Na]^+$: 2852.1254

UV-Vis λ (M^{-1} cm^{-1}) 298 nm (140000), 497 nm (180000), 534 nm (210000)

CHN theoretical (%) C: 74.66, H: 5.84, N: 5.94; found (%) C: 74.34; H: 5.68; N: 5.80

3. ^{1}H & ^{13}C NMR Spectroscopy

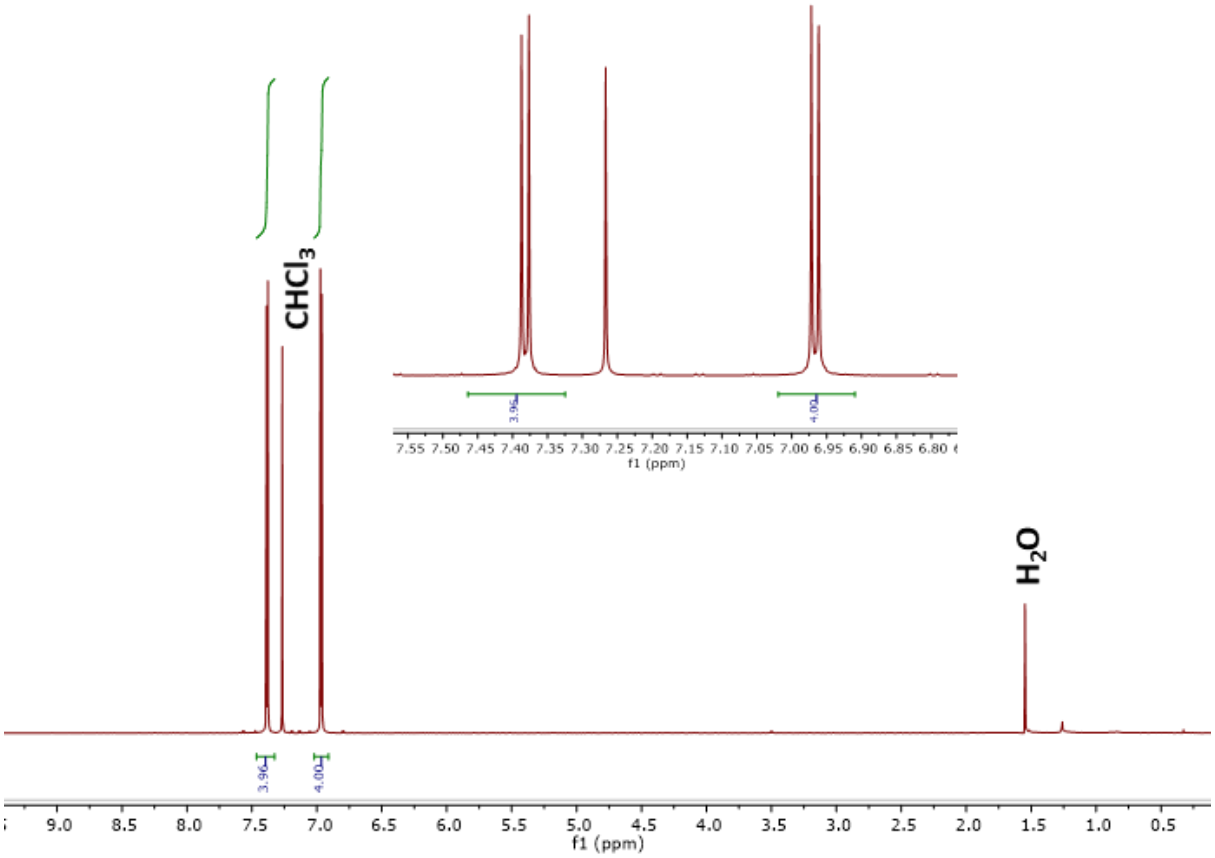

Figure S1. ^{1}H NMR spectrum of Th_4 (500 MHz, $CDCl_3$).

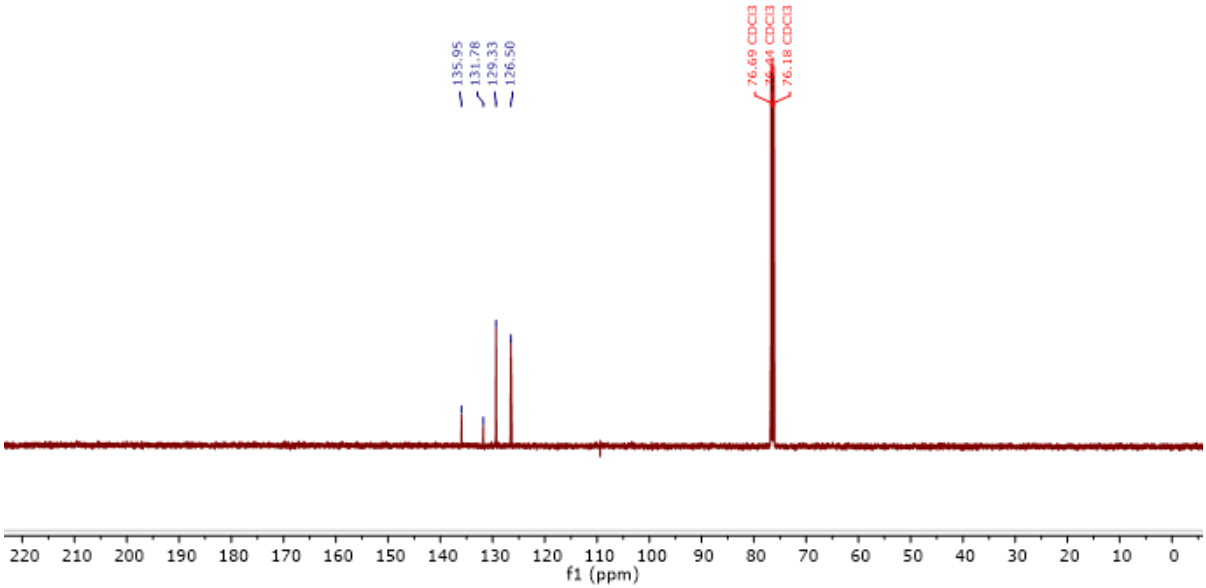

Figure S2. ^{13}C NMR spectrum of Th_4 (126 MHz, $CDCl_3$).

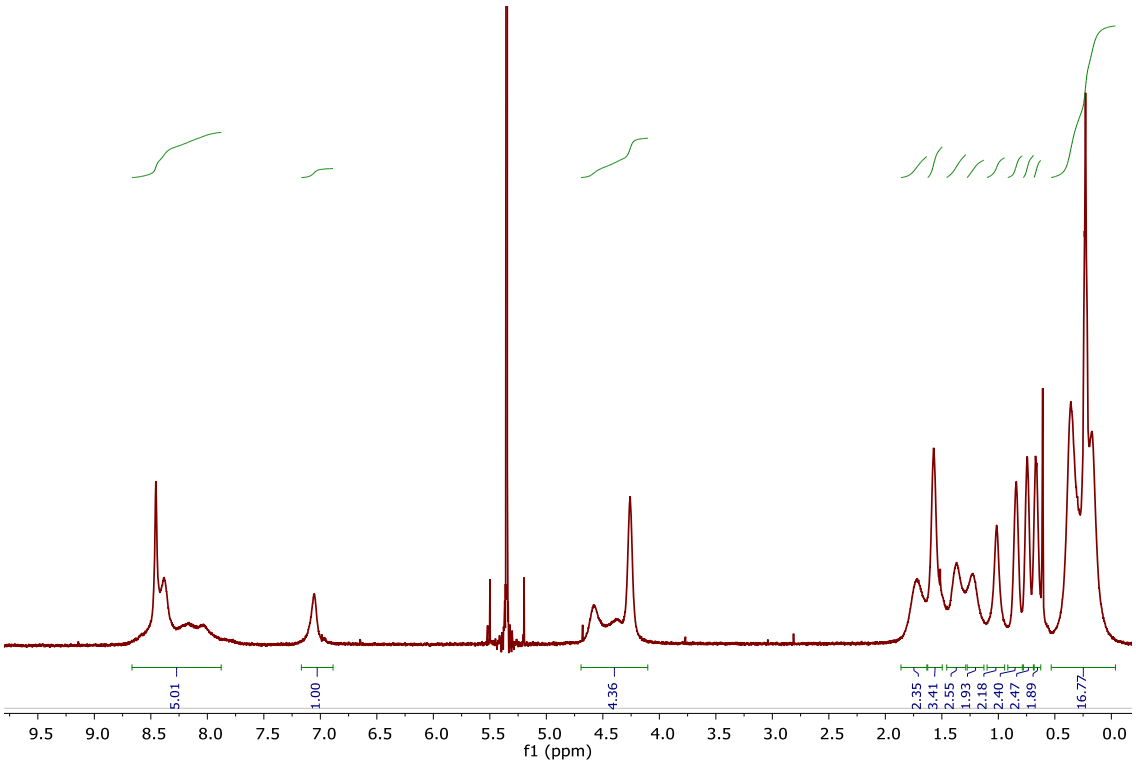

Figure S3. ^{1}H NMR spectrum of Th_4PDI_4 (600 MHz, tetrachloroethane-d_2, 20 ºC).

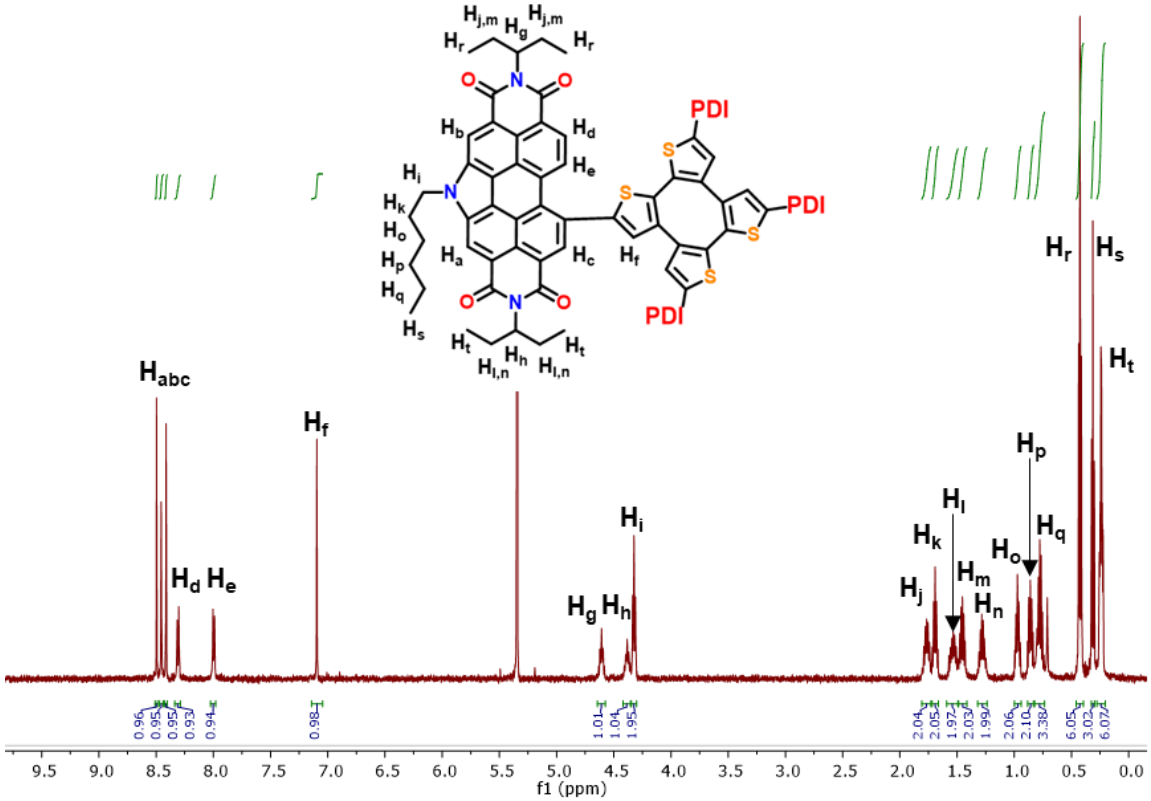

Figure S4. ^{1}H NMR spectrum of Th_4PDI_4 (600 MHz, tetrachloroethane-d_2, 120 ºC).

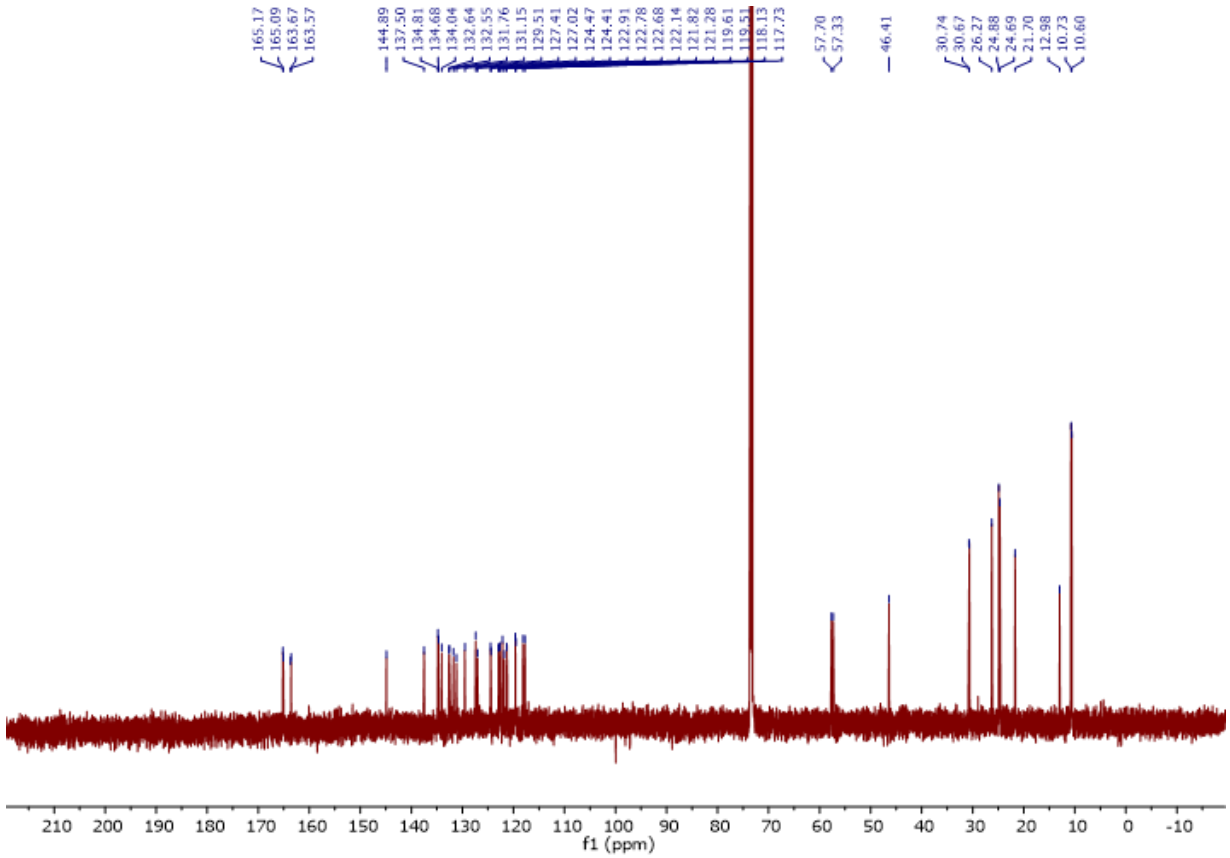

Figure S5. ^{13}C NMR spectrum of Th_4PDI_4 (151 MHz, tetrachloroethane-d_2, 120 ºC).

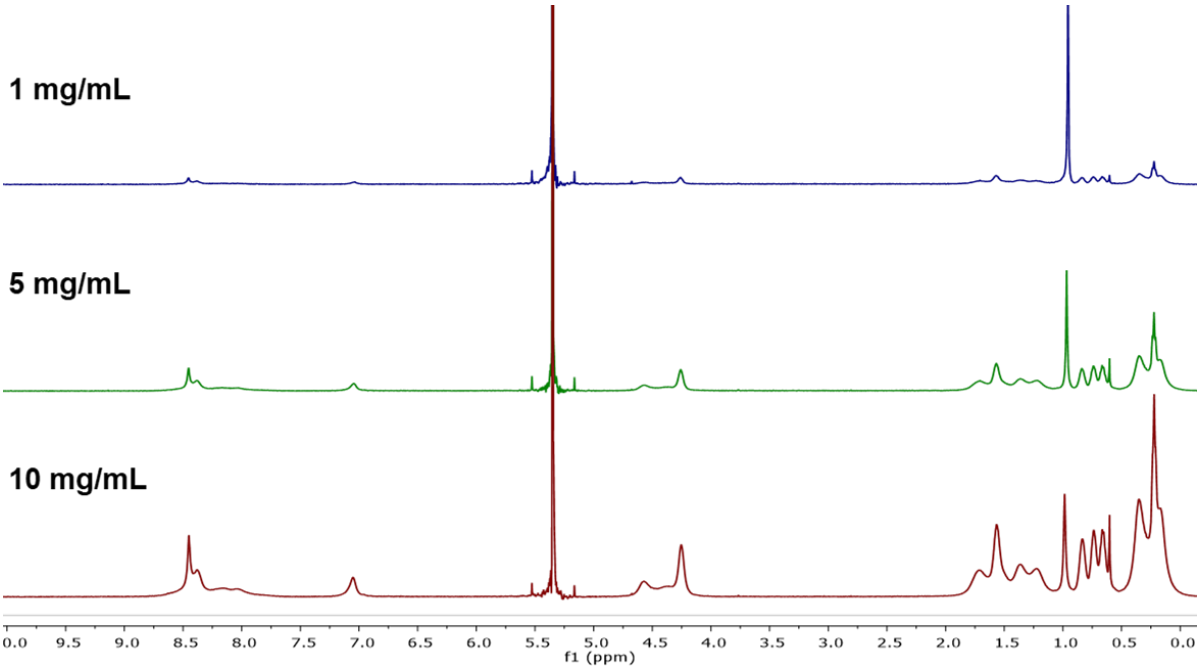

Figure S6. Concentration-dependent ^{1}H NMR spectra of Th_4PDI_4 (600 MHz, tetrachloroethane-d_2, 20 ºC).

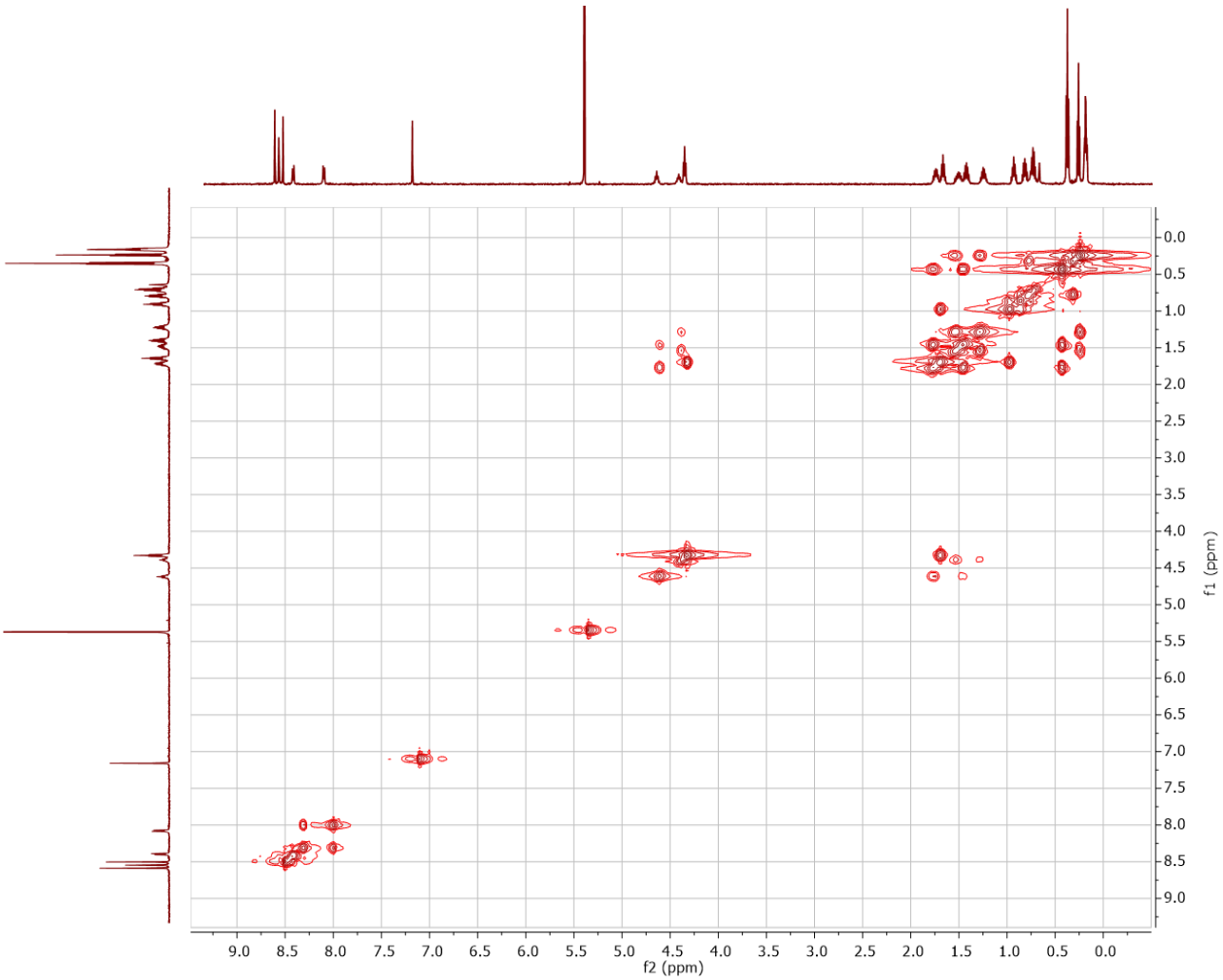

Figure S7. ^{1}H-^{1}H COSY spectrum of Th_4PDI_4 (600 MHz, tetrachloroethane-d_2, 120 ºC).

4. HR-MALDI-TOF

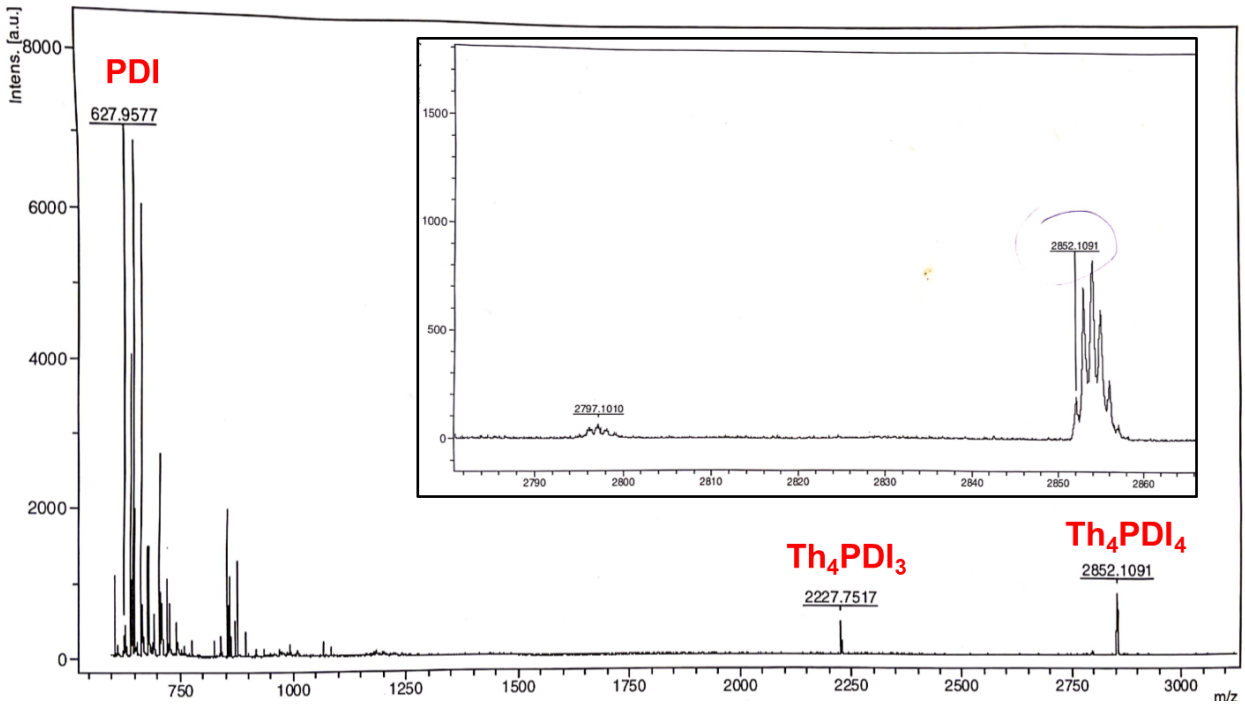

Figure S8. HR-MALDI-TOF mass spectrum showing incomplete substitution of Th_4 core.

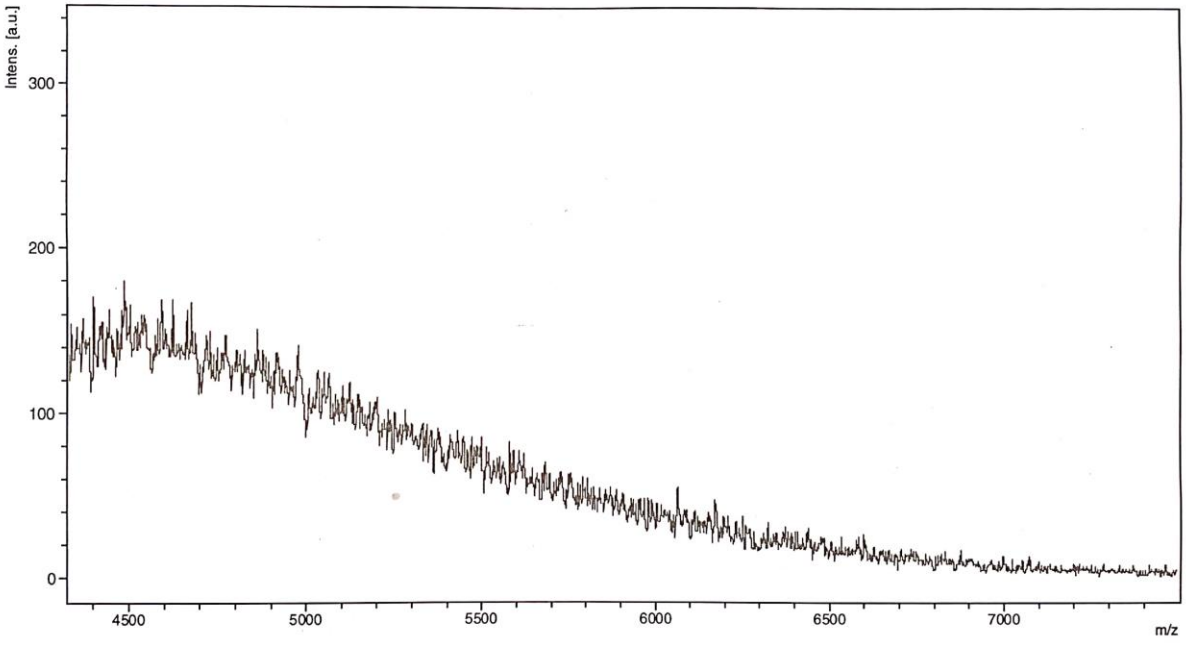

Figure S9. HR-MALDI-TOF mass spectrum showing no formation of Th_4PDI_8.

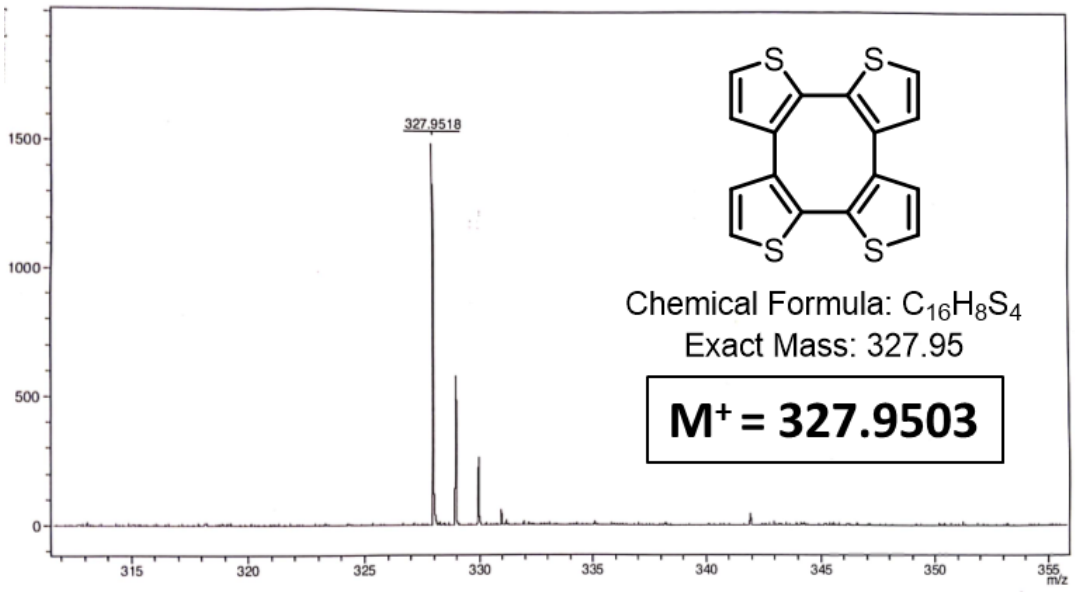

Figure S10. HR-MALDI-TOF mass spectrum of Th_4.

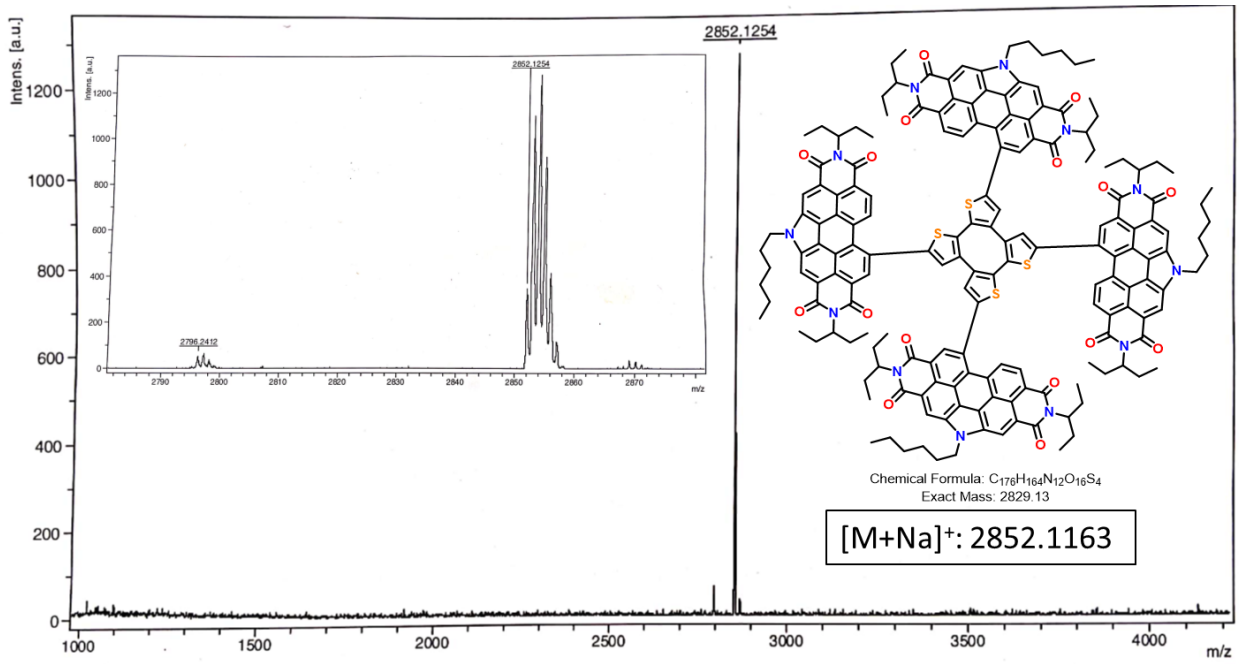

Figure S11. HR-MALDI-TOF mass spectrum of purified Th_4PDI_4.

5. Elemental Analysis & Thermal Properties

University of Calgary
Department of Chemistry EA Date: 7/24/2019

Name:	JOSH	Group:	GW
Sample:	Th_4PDI_4	Weight (mg):	1.527
%C (Actual):	74.34	%C (Theorectical):	74.66
%H (Actual):	5.68	%H (Theoretical):	5.84
%N (Actual):	5.80	%N (Theoretical):	5.94

Figure S12. CHN elemental analysis of Th_4PDI_4.

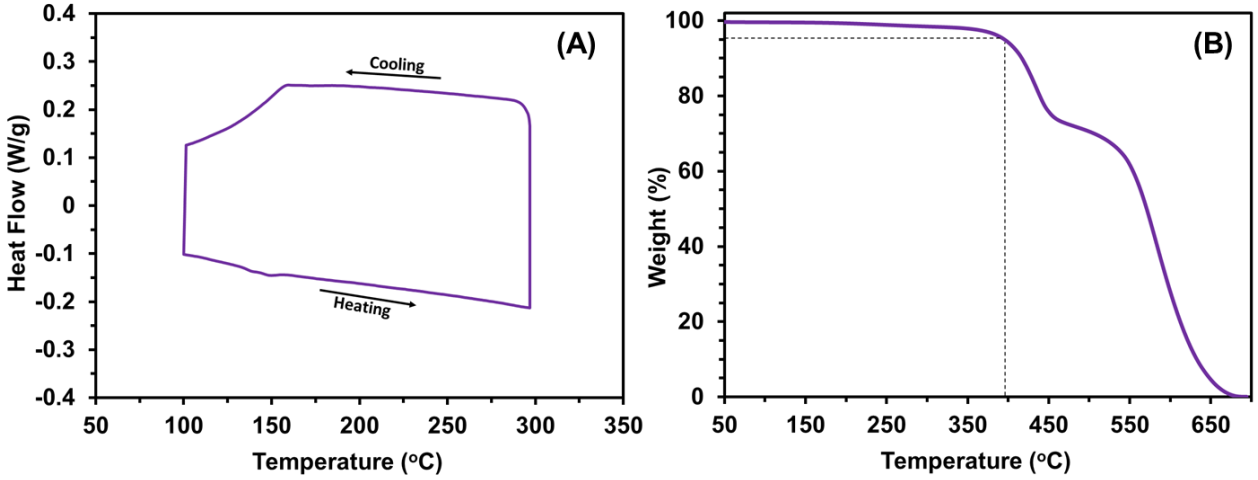

Figure S13. Differential scan calorimetry (A) and thermal gravimetric analysis (B) profiles of Th_4PDI_4. All features observed in the DSC trace of Th_4PDI_4 near 150 ºC are artifacts of the instrument, as they were also observed in the blank.

6. UV-Visible Spectroscopy & X-Ray Diffraction

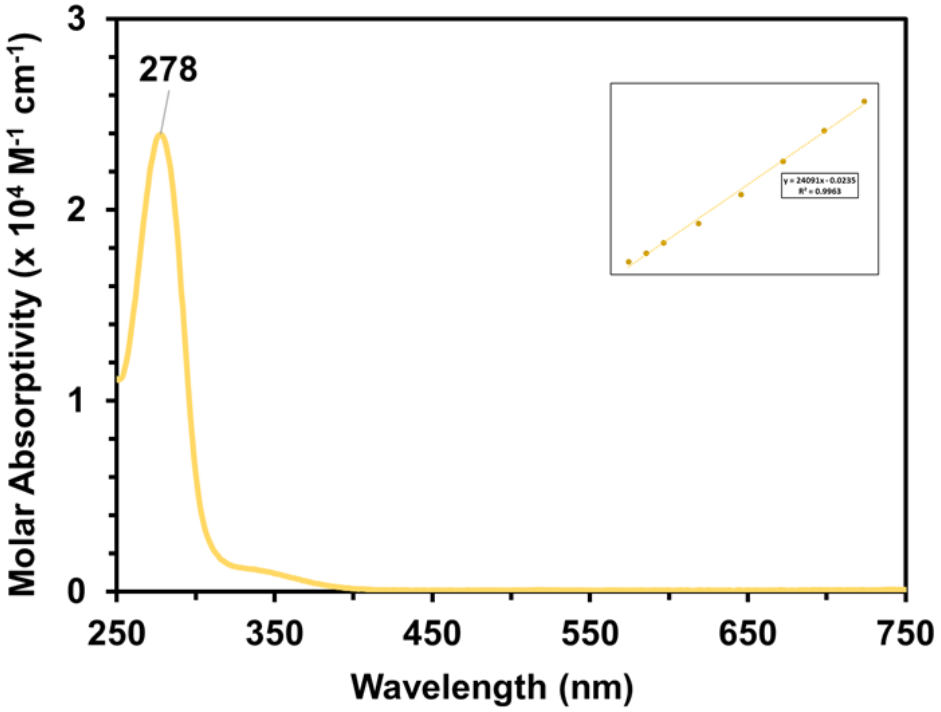

Figure S14. UV-visible absorption spectrum of Th_4 in $CHCl_3$, with calibration curve inset.

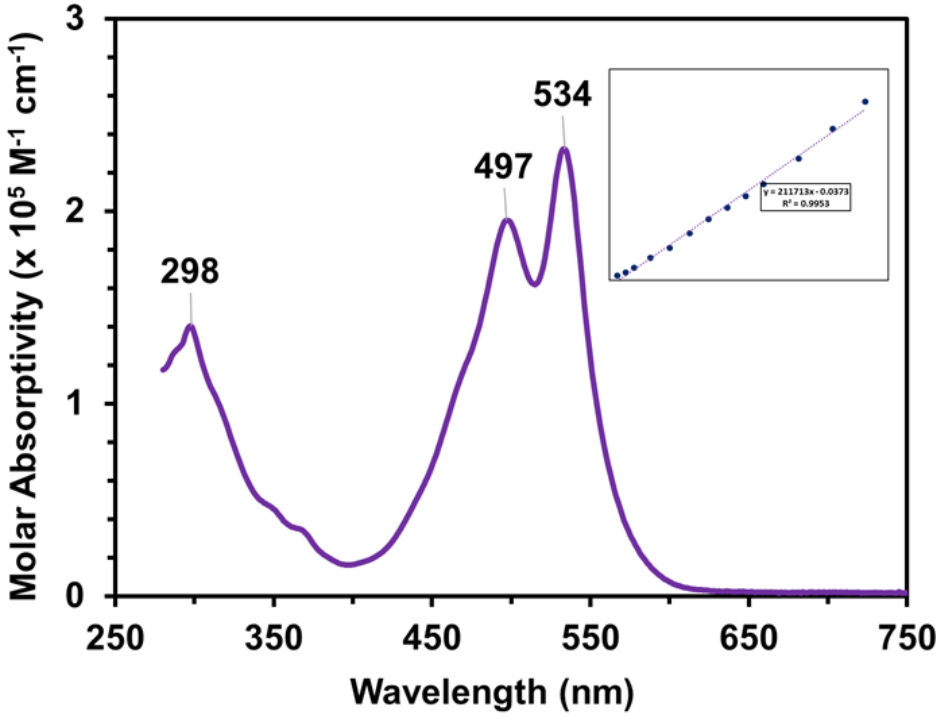

Figure S15. UV-visible absorption spectrum of Th_4PDI_4 in $CHCl_3$, with calibration curve inset.

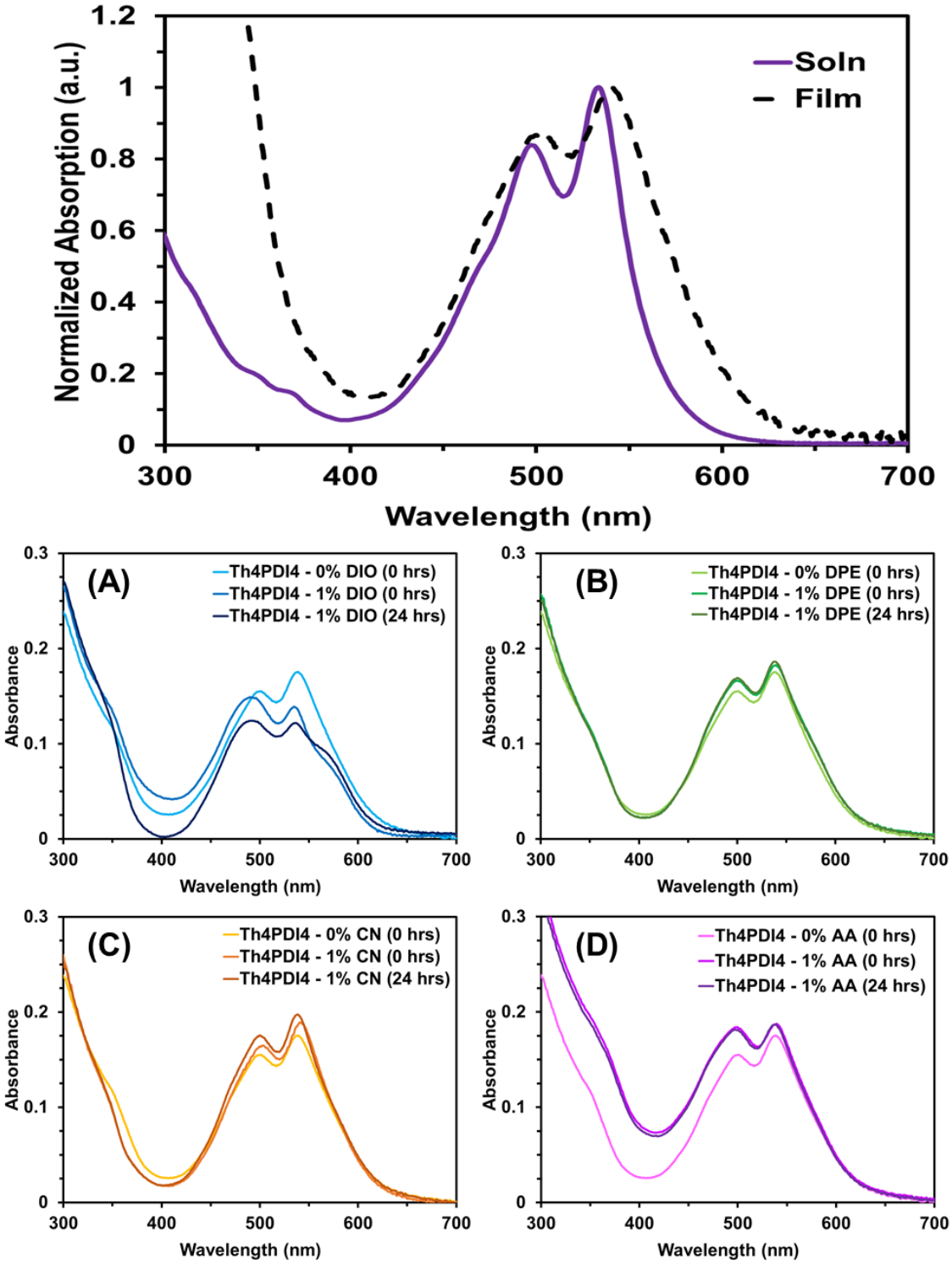

Figure S16. Directly comparing the UV-vis absorption spectra of Th_4PDI_4 in solution (*o*-DCB) and in thin film. The influence of 1,8-diiodooctane (A), diphenyl ether (B), chloronaphthalene (C), and *p*-anisaldehyde (D) on the thin film UV-vis absorption spectra of Th_4PDI_4 are also depicted.

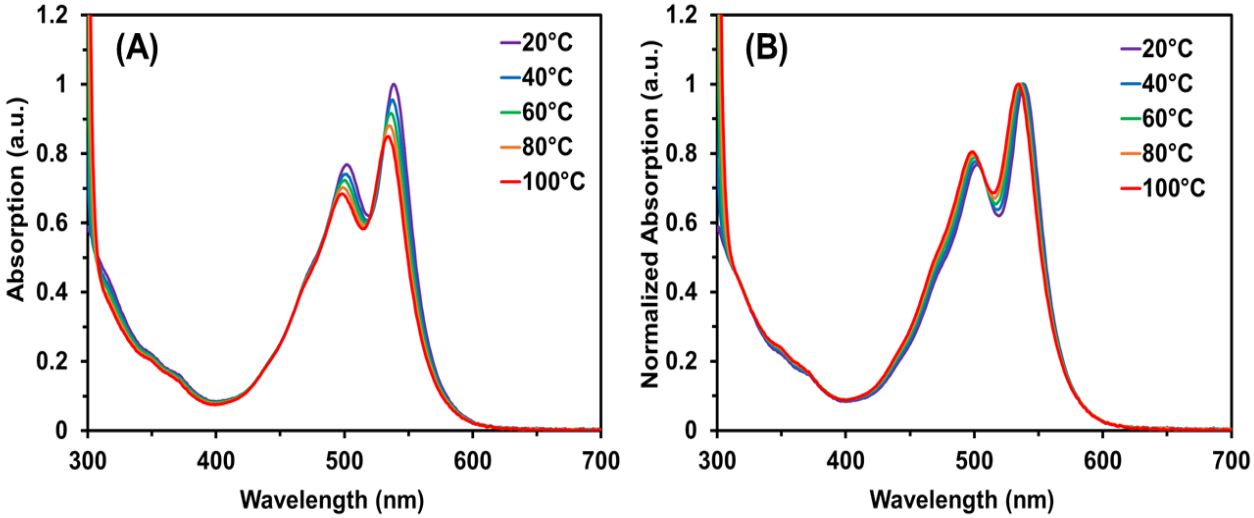

Figure S17. The raw (A) and normalized (B) variable-temperature UV-vis absorption spectra of Th_4PDI_4 (10^{-5} M in *o*-DCB).

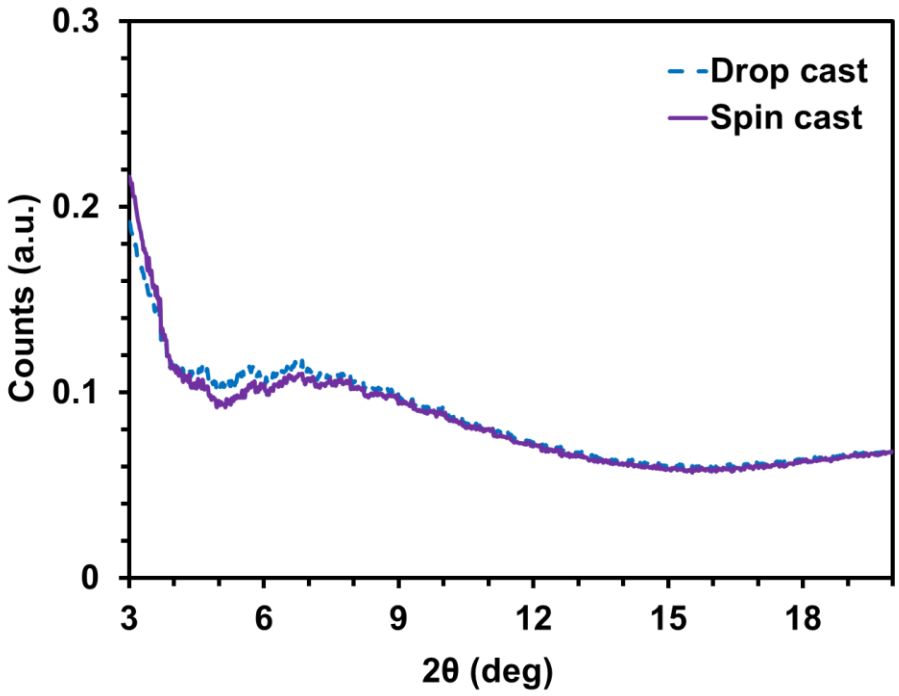

Figure S18. X-ray diffraction spectra of drop cast and spin cast Th_4PDI_4 thin films.

7. Voltammetry

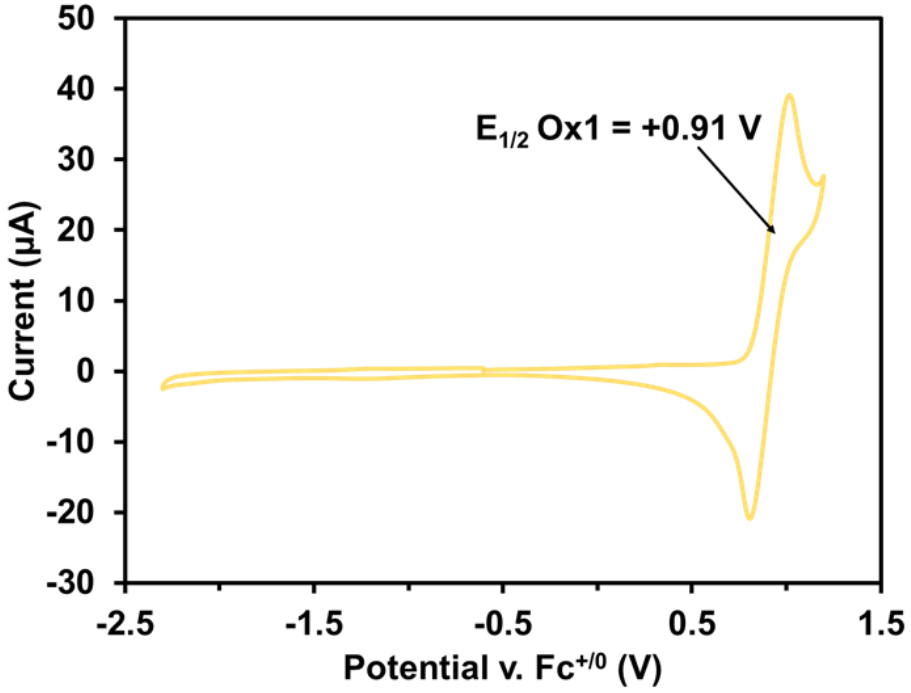

Figure S19. Cyclic voltammogram of Th_4 (~1 mM) in CH_2Cl_2, recorded at 100 mV/s.

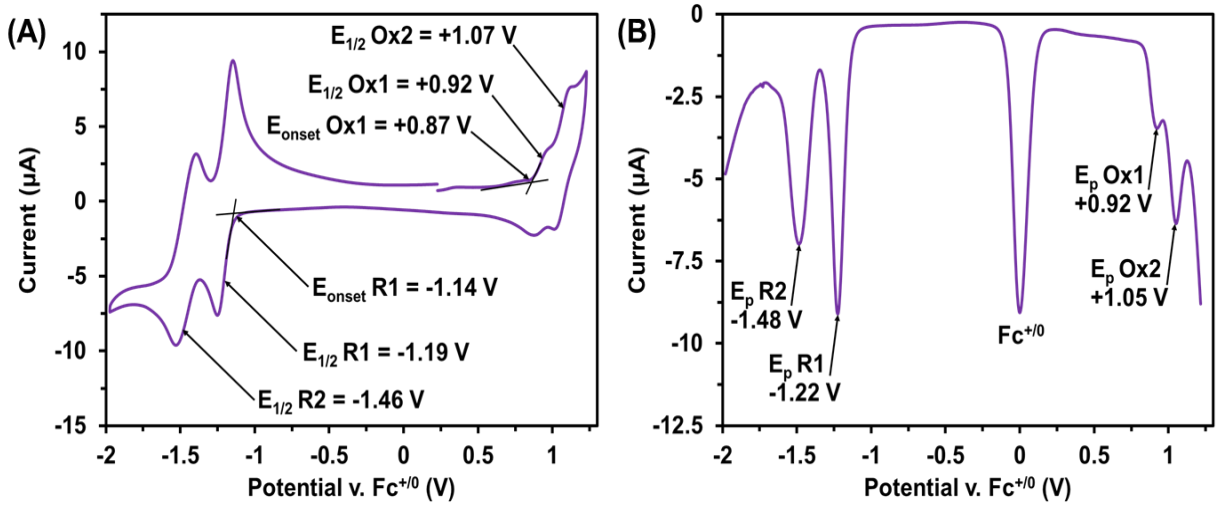

Figure S20. Cyclic voltammogram (A) and differential pulse voltammogram (B) of Th_4PDI_4 (~1 mM) in CH_2Cl_2, recorded at 100 mV/s.

8. Density Functional Theory

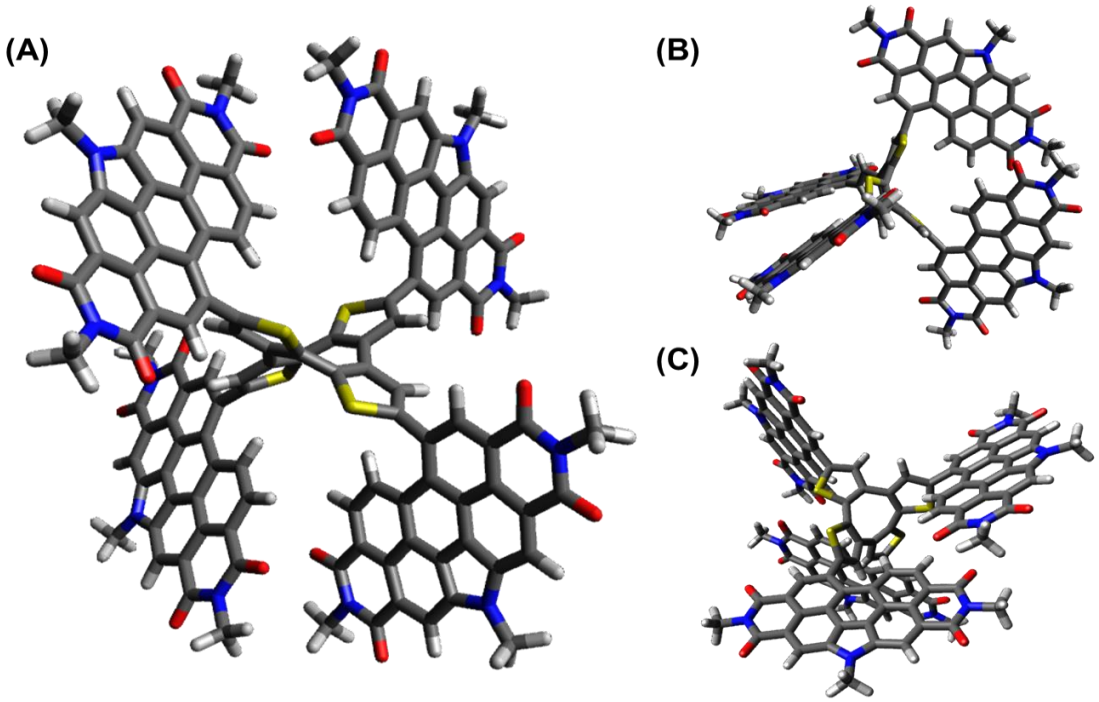

Figure S21. Optimized geometry of Th_4PDI_4 at B3LYP/6-31G(d,p) ground-state.

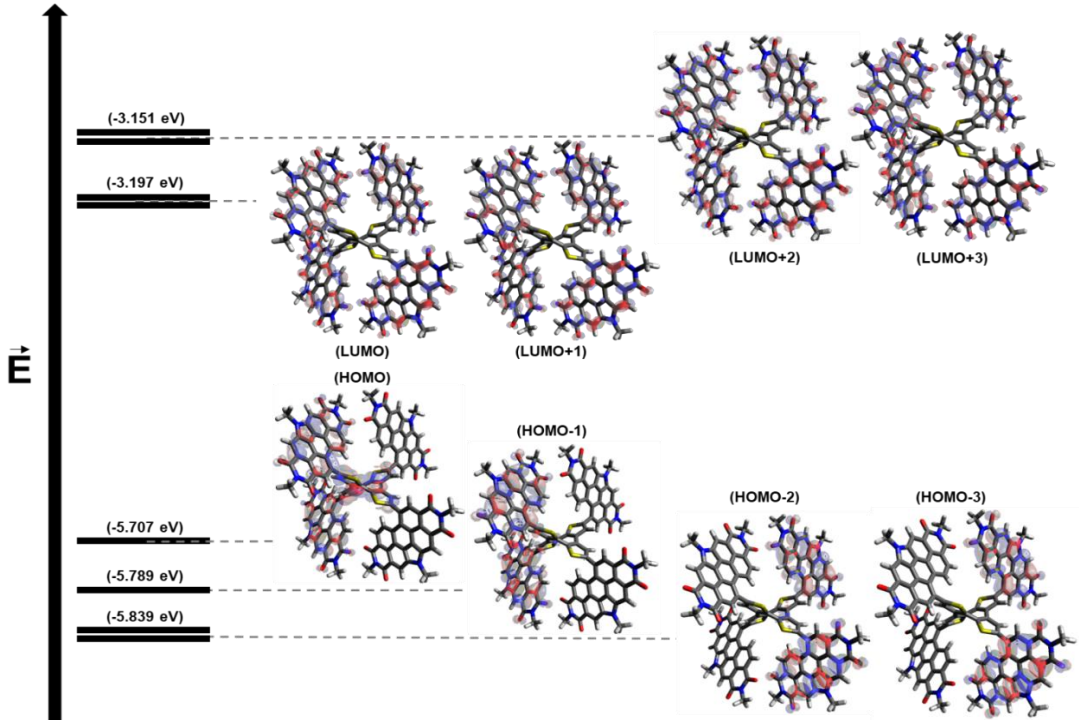

Figure S22. Molecular orbital diagram of Th_4PDI_4 at B3LYP/6-31G(d,p) ground-state. Depicted energy-levels represent DFT calculated values, rather than experimentally determined values.

9. OPV Device Optimization

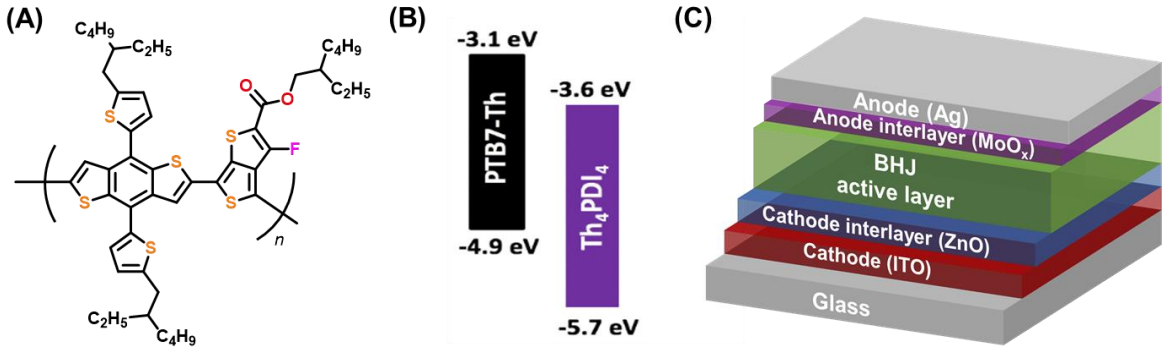

Figure S23. Chemical structure of PTB7-Th (A), CV determined energy levels (using $E_{1/2}$) for PTB7-Th and Th_4PDI_4 (B), and proof-of-concept OPV device architecture (C).

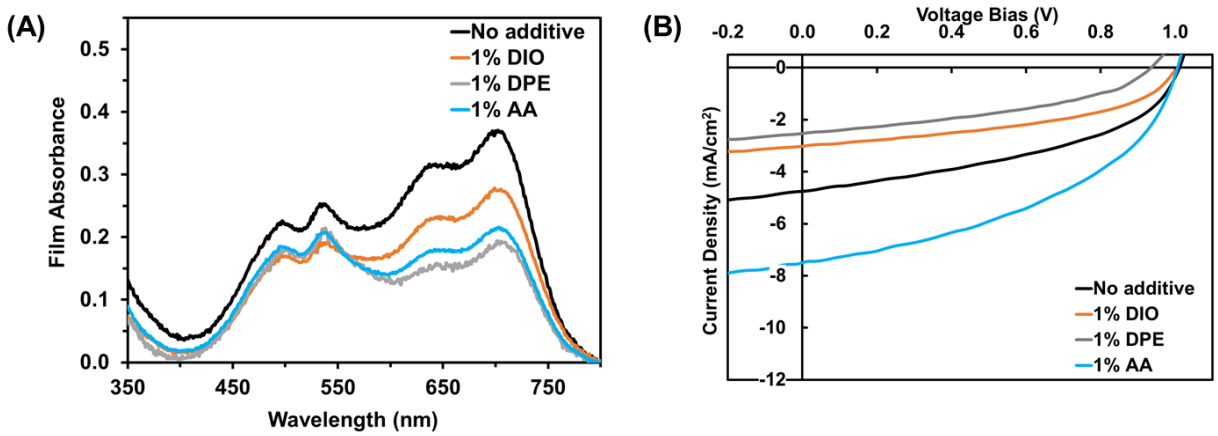

Figure S24. UV-visible spectra (A) and J-V curves (B) of 1 :1 PTB7-Th:Th_4PDI_4 films and devices, respectively, spin-coated from *o*-DCB containing 0 or 1% (v/v) of DIO, DPE or AA.

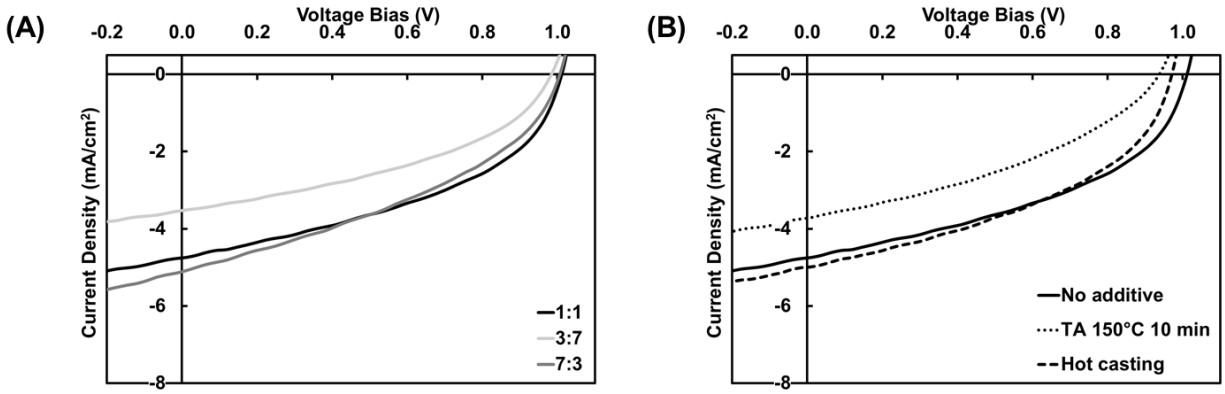

Figure S25. J-V curves of the PTB7-Th-Th_4PDI_4 devices spin-coated from *o*-DCB using different (A) donor:acceptor weight ratio and (B) different processing.

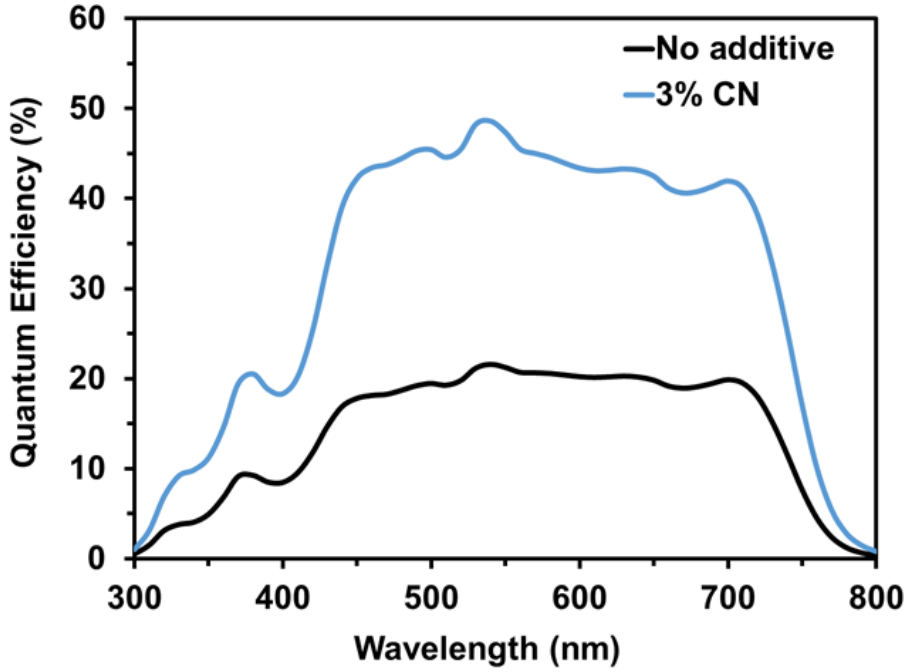

Figure S26. External quantum efficiency of 1:1 PTB7-Th:Th_4PDI_4 films spin-coated from *o*-DCB containing 0 or 3% (v/v) CN.

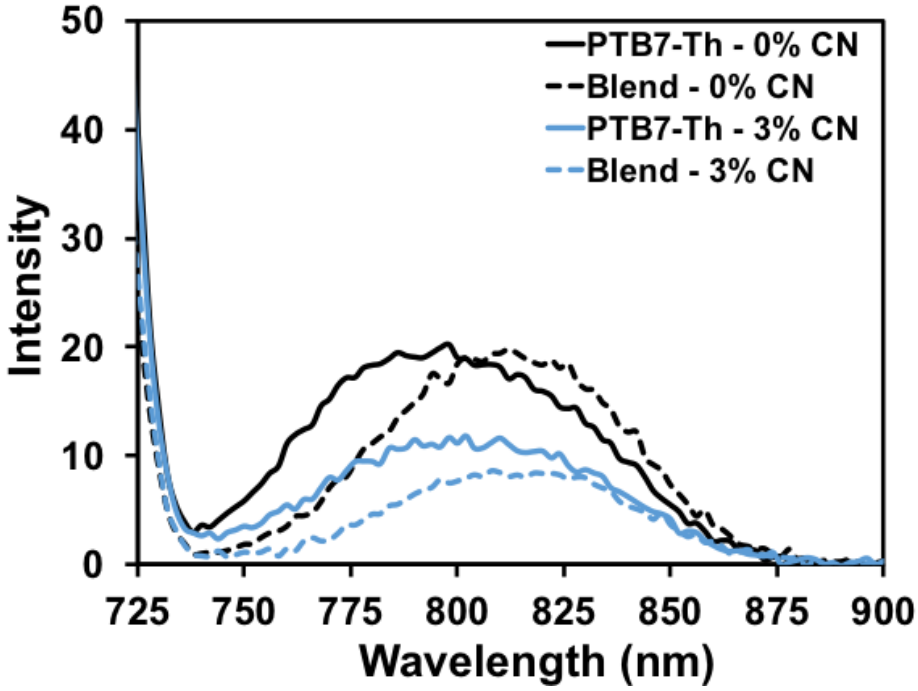

Figure S27. Photoluminescence spectra of PTB7-Th and of 1:1 PTB7-Th:Th_4PDI_4 films spin-coated from *o*-DCB containing 0 or 3% (v/v) CN. The excitation wavelength is 705 nm.

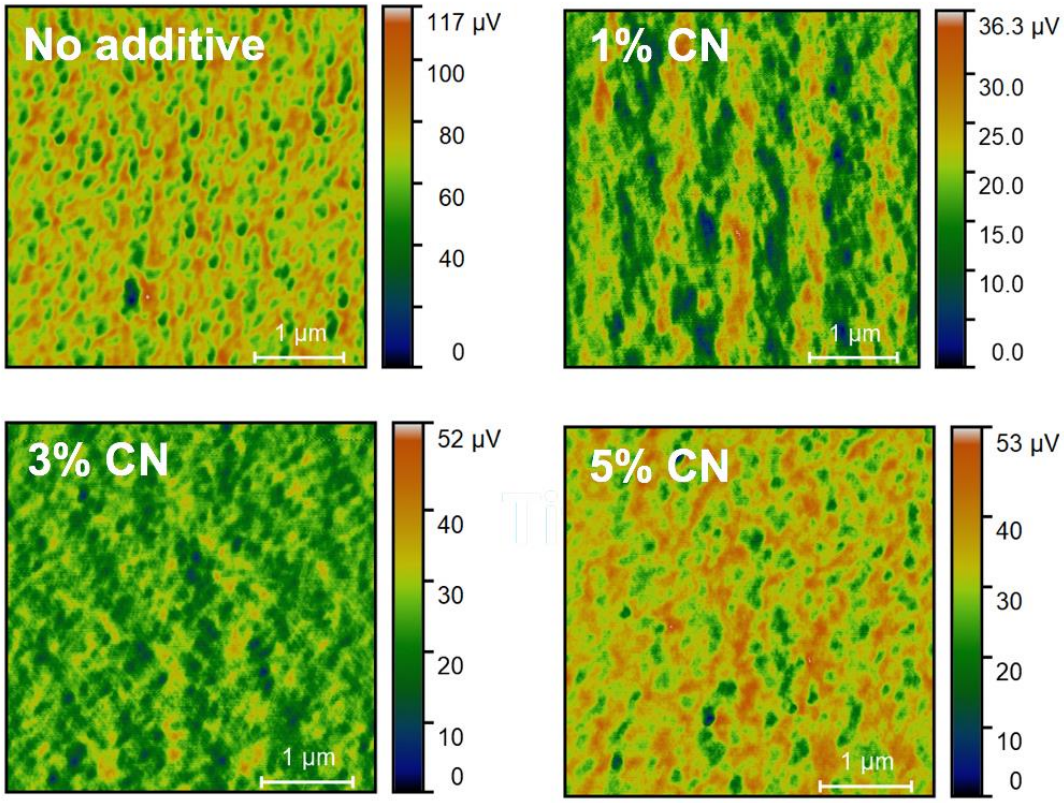

Figure S28. AFM phase images of the 1:1 PTB7-Th:Th_4PDI_4 films spin-coated from *o*-DCB containing 0, 1, 3 or 5% (v/v) CN.

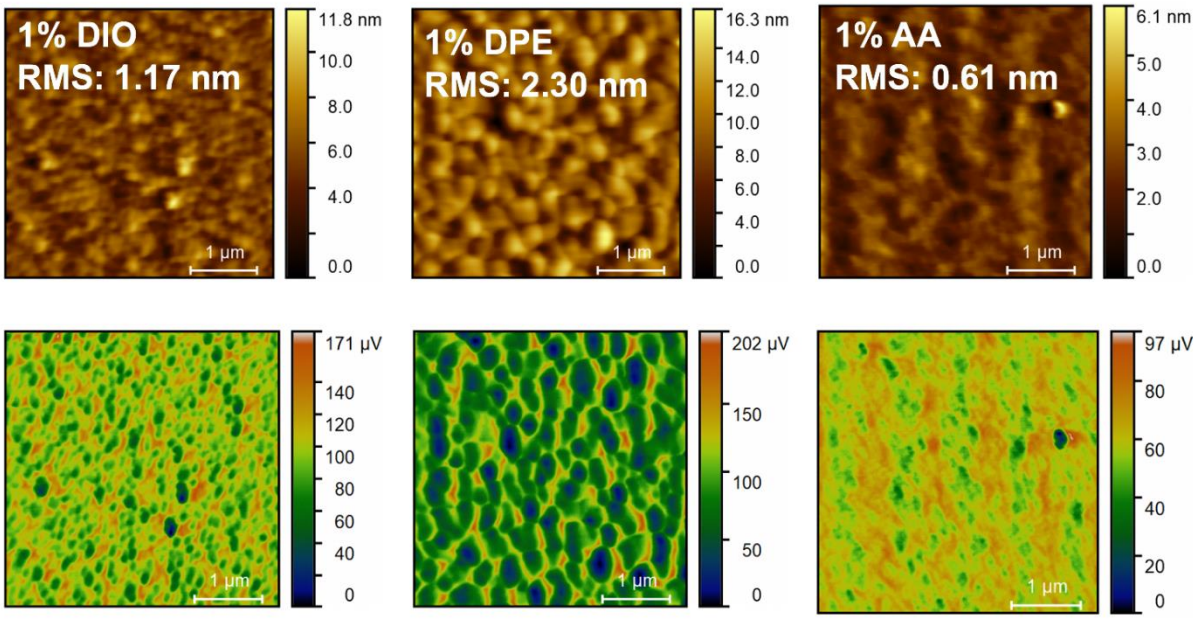

Figure S29. AFM height (top) and phase (bottom) images of the PTB7-Th:Th_4PDI_4 devices spin-coated from *o*-DCB using different processing conditions.

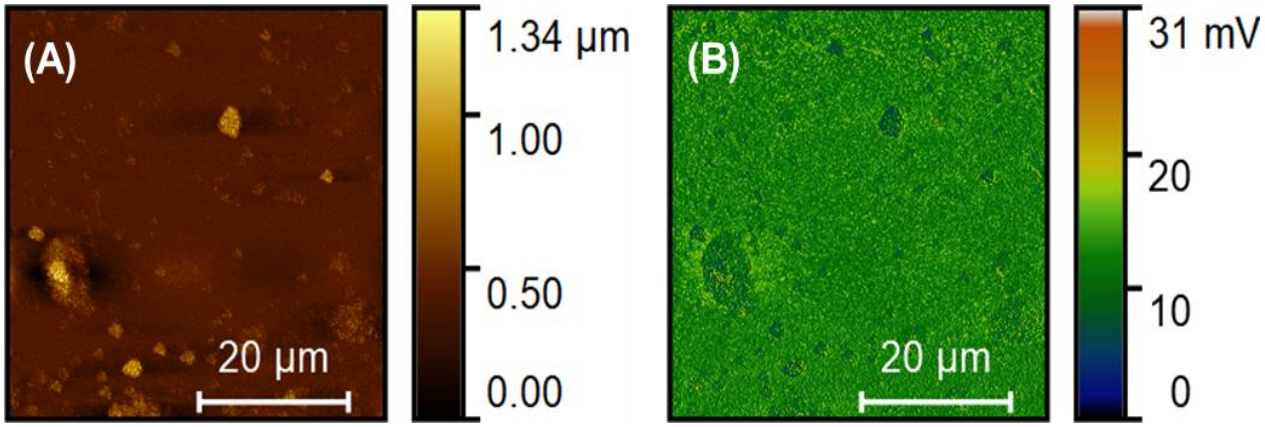

Figure S30. AFM height (A) and phase (B) images of the PTB7-Th:Th_4PDI_4 devices spin-coated from *o*-DCB using 3 % (v/v) CN. The calculated film RMS was 74 nm.

Table S1. OPV data of PTB7-Th:**Th_4PDI_4** blends spin-coated from *o*-DCB with different additives. Best PCE results are highlighted in bold. Averages are in italics.

Active layer	**V_{oc} (V)**	**J_{sc} (mA/cm^2)**	**FF (%)**	**PCE (%)**
***o*-DCB, 15 mg/mL, 1:1 ratio**				
No additive	1.00	4.3	40	1.72
	1.02	**5.1**	**42**	**2.20**
	1.02	4.8	43	2.10
	1.01	4.7	44	2.10
	1.03	3.8	43	1.68
	1.01	4.3	40	1.72
	1.01	4.4	39	1.73
	1.01	*4.5*	*42*	*1.89*
1% (v/v) DIO	1.01	3.0	46	1.39
	1.01	3.0	45	1.36
	1.03	2.9	44	1.31
	1.01	2.9	45	1.30
	1.04	**3.6**	**45**	**1.67**
	1.02	3.6	44	1.63
	1.02	*3.2*	*45*	*1.44*
1% (v/v) DPE	**0.97**	**2.6**	**40**	**1.02**
	0.93	2.5	40	0.95
	0.91	2.5	43	0.99
	0.94	*2.6*	*41*	*0.99*
1% (v/v) AA	0.98	6.9	40	2.72
	1.00	**8.1**	**44**	**3.53**
	1.00	7.5	44	3.32
	1.00	7.4	44	3.27
	1.00	*7.5*	*43*	*3.21*

1% (v/v) CN	0.97	9.6	37	3.51
	0.97	9.4	39	3.50
	0.96	8.9	35	3.00
	1.00	8.8	38	3.32
	0.98	9.0	38	3.34
	0.98	**9.5**	**39**	**3.61**
	0.99	9.1	39	3.51
	0.99	9.4	38	3.54
	0.98	*9.2*	*38*	*3.42*
3% (v/v) CN	0.99	10.7	41	4.32
	0.99	**10.6**	**43**	**4.52**
	0.99	10.3	42	4.33
	0.98	10.6	40	4.15
	0.99	10.4	42	4.36
	0.99	10.2	42	4.21
	1.00	8.8	45	3.93
	0.99	*10.2*	*42*	*4.26*
5% (v/v) CN	0.99	9.6	41	3.89
	1.00	9.2	44	4.10
	1.00	**9.3**	**45**	**4.16**
	0.98	9.3	42	3.82
	0.99	*9.4*	*43*	*3.99*
Thermal annealing, 150°C, 10 min	**0.94**	**4.0**	**37**	**1.40**
	0.93	3.6	38	1.28
	0.93	3.7	38	1.31
	0.92	3.9	38	1.36
	0.91	3.5	38	1.22
	0.93	*3.8*	*38*	*1.31*
Hot casting 100°C	**0.97**	**5.8**	**42**	**2.36**
	0.97	5.0	43	2.06
	0.97	5.1	42	2.09
	0.99	4.0	41	1.63
	0.98	*5.0*	*42*	*2.03*
***o*-DCB, 15 mg/mL, 3:7 ratio**				
No additive	**0.97**	**3.7**	**42**	**1.50**
	0.98	3.4	41	1.40
	0.98	3.5	41	1.43
	0.97	3.4	37	1.22
	0.99	3.1	41	1.24
	0.97	3.1	41	1.25
	0.98	*3.4*	*40*	*1.34*
***o*-DCB, 15 mg/mL, 7:3 ratio**				
No additive	**1.00**	**5.3**	**40**	**2.12**
	1.00	5.1	39	1.98
	1.01	4.8	39	1.90
	0.99	5.1	39	1.99
	0.99	5.0	39	1.96
	0.99	5.1	41	2.05
	1.00	*5.1*	*40*	*2.00*

10. References

(1) Pommerehne, J.; Vestweber, H.; Guss, W.; Mahrt, R. F.; Bässler, H.; Porsch, M.; Daub, J. Efficient Two Layer Leds on a Polymer Blend Basis. *Adv. Mater.* **1995**, *7* (6), 551–554. https://doi.org/10.1002/adma.19950070608.

(2) Sun, Y.; Seo, J. H.; Takacs, C. J.; Seifter, J.; Heeger, A. J. Inverted Polymer Solar Cells Integrated with a Low-Temperature-Annealed Sol-Gel-Derived ZnO Film as an Electron Transport Layer. *Adv. Mater.* **2011**, *23* (14), 1679–1683. https://doi.org/10.1002/adma.201004301.

(3) Frisch, M. J.; Trucks, G. W.; Schlegel, H. B.; Scuseria, G. E.; Robb, M. A.; Cheeseman, J. R.; Scalmani, G.; Barone, V.; Petersson, G. A.; Nakatsuji, H.; Li, X.; Caricato, M.; Marenich, A. V.; Bloino, J.; Janesko, B. G.; Gomperts, R.; Mennucci, B.; Hratchian, H. P.; Ortiz, J. V.; Izmaylov, A. F.; Sonnenberg, J. L.; Williams-Young, D.; Ding, F.; Lipparini, F.; Egidi, F.; Goings, J.; Peng, B.; Petrone, A.; Henderson, T.; Ranasinghe, D.; Zakrzewski, V. G.; Gao, J.; Rega, N.; Zheng, G.; Liang, W.; Hada, M.; Ehara, M.; Toyota, K.; Fukuda, R.; Hasegawa, J.; Ishida, M.; Nakajima, T.; Honda, Y.; Kitao, O.; Nakai, H.; Vreven, T.; Throssell, K.; Montgomery, J. A., Jr.; Peralta, J. E.; Ogliaro, F.; Bearpark, M. J.; Heyd, J. J.; Brothers, E. N.; Kudin, K. N.; Staroverov, V. N.; Keith, T. A.; Kobayashi, R.; Normand, J.; Raghavachari, K.; Rendell, A. P.; Burant, J. C.; Iyengar, S. S.; Tomasi, J.; Cossi, M.; Millam, J. M.; Klene, M.; Adamo, C.; Cammi, R.; Ochterski, J. W.; Martin, R. L.; Morokuma, K.; Farkas, O.; Foresman, J. B.; Fox, D. J Gaussian 09 Revis. E01 Gaussian Inc Wallingford CT.

(4) Wanwong, S.; Poe, A.; Balaji, G.; Thayumanavan, S. The Effect of Heteroatom Conformation on Optoelectronic Properties of Cyclopentadithiophene Derivatives. *Org. Biomol. Chem.* **2014**, *12* (15), 2474–2478. https://doi.org/10.1039/C3OB41648H.

(5) Mora, J. U.; Garcia, I.; Zimmermann, I.; Aragó, J.; Calbo, J.; Grancini, G.; Ontoria, A. M.; Orti, E.; Martín, N.; Nazeeruddin, M. K. Saddle-like, π–Conjugated, Cyclooctatetrathiophene-Based, Hole-Transporting Material for Perovskite Solar Cells. *J. Mater. Chem. C* **2019**. https://doi.org/10.1039/C9TC00437H.

(6) Wang, Y.; Wang, Z.; Zhao, D.; Wang, Z.; Cheng, Y.; Wang, H. Efficient Synthesis of Trimethylsilyl-Substituted Dithieno[2,3-b:3′,2′-d]Thiophene, Tetra[2,3-Thienylene] and Hexa[2,3-Thienylene] from Substituted [3,3′]Bithiophenyl. *Synlett* **2007**, *2007* (15), 2390–2394. https://doi.org/10.1055/s-2007-985582.

(7) Hendsbee, A. D.; Sun, J.-P.; Law, W. K.; Yan, H.; Hill, I. G.; Spasyuk, D. M.; Welch, G. C. Synthesis, Self-Assembly, and Solar Cell Performance of N-Annulated Perylene Diimide Non-Fullerene Acceptors. *Chem. Mater.* **2016**, *28* (19), 7098–7109. https://doi.org/10.1021/acs.chemmater.6b03292.